DOI: 10.1002/adma.200601437

Self-Organization and Nanoscale Electronic Properties of Azatriphenylene-Based Architectures: A Scanning Probe Microscopy Study**

By *Matteo Palma*, *Jérémy Levin*, *Vincent Lemaur*, *Andrea Liscio*, *Vincenzo Palermo*, *Jérôme Cornil*, *Yves Geerts*, *Matthias Lehmann*, and *Paolo Samorì**

There is currently great interest in probing and gaining a better understanding of the nanometer-scale electronic properties of π-conjugated supramolecular architectures as spatially confined electrically active nano-objects.[1–3] It is clear that the performance of device prototypes based on an ensemble of molecules can be improved by achieving full control of the supramolecular self-organization of the active organic components, and by elucidating and optimizing many other physicochemical properties, such as their complex electronic structure, both at the single-molecule and supramolecular level. In this context, scanning probe microscopy (SPM) offers direct, yet quantitative, mapping of a variety of physicochemical properties with submolecular resolution.[4]

Conjugated discotic systems are unique building blocks for (opto)electronic applications.[5] Columnar nanostructures made up through π–π stacking of alkylated discotic building blocks are interesting, both as nanowires[5–7], and as molecular systems forming (uniform) films with a high degree of molecular orientation.[8,9] The increasing size of the disk leads, on one hand, to a moderate enhancement of the electronic function because of a greater delocalization of the π states, but on the other hand, it is accompanied by a drastic limitation in processability, both from solution and from vacuum sublimation.[5] In this context, medium-sized disks, such as triphenylene derivatives, represent very interesting discotic molecules, because the ease of substitution in the peripheral positions allows solution processability (and hence a high level of purification) and self-organization into columnar nanostructures possessing relatively high charge-carrier mobilities. This paves the way for their potential application as quasi-1D charge-carrier transporters for electrical conduction and photoconduction.[8,10]

Scanning tunneling microscopy (STM) has become a major tool for investigating the structure and electronic properties of single molecules forming 2D crystals on conductive substrates, such as highly oriented pyrolitic graphite (HOPG).[11–15] The self-assembly of alkylated triphenylenes on surfaces has been investigated primarily for physisorbed monolayers on HOPG,[16–18] and differences in the 2D ordering have been observed depending on the nature and length of the side chains.[16,18,19] So far, little is known about the self-organization on surfaces or the electronic properties of discotics incorporating heteroatoms, both in the conjugated cores, and/or in the sidechains.

In this Communication, we report on the structural and electronic properties of a specially designed and synthesized triphenylene derivative physisorbed on surfaces. Submolecularly resolved STM images at the solid/liquid interface, corroborated by quantum-chemical calculations, enabled us to shed light on both the monolayer packing and the electronic properties of this molecule with a submolecular resolution. Furthermore, Kelvin probe force microscopy (KPFM)[20] provided a quantitative insight into the electronic properties of dry architectures self-assembled on HOPG.

Among triphenylene derivatives,[21] hexaazatriphenylenes (HATs) have attracted considerable interest as potential electron carriers in view of the nature of their conjugated core. HAT derivatives are indeed made of strongly electron-deficient heterocycles: the presence of six nitrogen atoms in the aromatic core is expected to significantly increase the first reduction potential, thus facilitating charge injection.[22,23] Sur-

[*] Dr. P. Samorì, Dr. A. Liscio, Dr. V. Palermo
Istituto per la Sintesi Organica e la Fotoreattività
Consiglio Nazionale delle Ricerche
via Gobetti 101, 40129 Bologna (Italy)
E-mail: samori@isof.cnr.it
Dr. P. Samorì, M. Palma
Nanochemistry Laboratory
Institut de Science et d'Ingénierie Supramoléculaires (ISIS)
Université Louis Pasteur
8 allée Gaspard Monge, 67083 Strasbourg (France)
J. Levin, Prof. Y. Geerts, Dr. M. Lehmann
Laboratoire de Chimie des Polymères, CP 206/1
Université Libre de Bruxelles
Boulevard du Triomphe, 1050 Bruxelles (Belgium)
Dr. V. Lemaur, Dr. J. Cornil
Service de Chimie des Matériaux Nouveaux,
Université de Mons-Hainaut
Place du Parc 20, 7000 Mons (Belgium)
Dr. M. Lehmann
Institut für Chemie
Technische Universität Chemnitz
Straße der Nationen 62, 09111 Chemnitz (Germany)

[**] Financial support from the EU through the Marie Curie EST project SUPER (MEST-CT-2004-008128) and IP-NAIMO (NMP4-CT-2004-500355), the Regione Emilia-Romagna PRIITT Nanofaber Net-Lab, the ERA-Chemistry project SurConFold, and the Bundesministerium für Bildung und Forschung (BMBF) are gratefully acknowledged. The work in Mons is partly supported by the Belgian Federal Government "Interuniversity Attraction Pole in Supramolecular Chemistry and Catalysis, PAI 5/3" and the Belgian National Fund for Scientific Research (FNRS). J. C. is an FNRS Research Associate.

ADVANCED MATERIALS

prisingly, hexathialkylhexaazatriphenylenes do not form columnar liquid-crystalline phases like their corresponding triphenylene derivatives, probably because of the large negative charges on the nitrogen atoms, which lead to the repulsion of the adjacent cores.[24] Hydrogen bonds were used to counterbalance and overcome this Coulombic repulsion, leading to the formation of a discotic mesophase with high charge-carrier mobility (up to ca. 0.1 $cm^2 V^{-1} s^{-1}$, as determined by microwave conductivity measurements).[25] Bearing this in mind, we designed and synthesized molecule **1** (Fig. 1) whose branched alkyl substitution was expected to provide good solubility in organic solvents. As in the case of other *N*-(alkyl)-substituted hexacarboxamidohexaazatriphenylene derivatives, the peculiar design of **1** gives various possibilities for intramolecular and intermolecular hydrogen bonds, as depicted in Figure 1. The intermolecular hydrogen bonding should optimize the stacking towards a cofacial configuration that maximizes the amplitude of the intermolecular transfer integral, as demonstrated by quantum-chemical calculations;[26] in turn, this should affect the rate of charge hopping, and hence the mobility values.

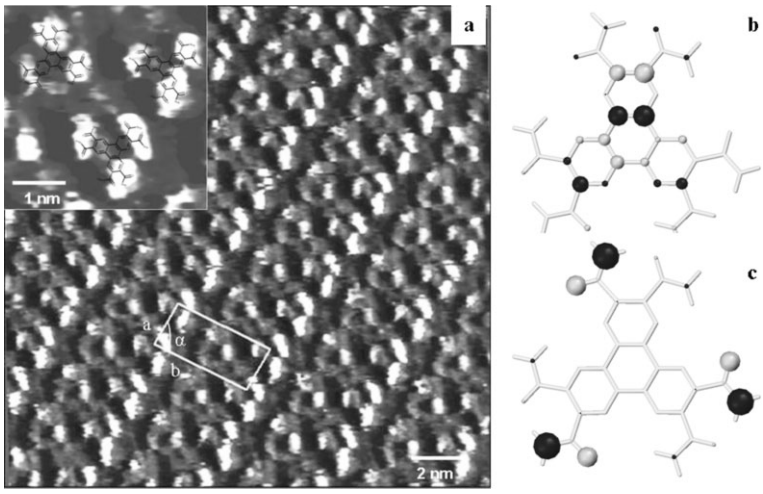

Figure 2. a) An STM image in constant height mode of **1** at the tetradecane/HOPG interface, recorded with a tip bias (V_t) = 450 mV and an average tunneling current (I_t) = 50 pA. The inset shows a magnified image of the dimers on which the molecular structure has been superimposed. b,c) HF/6-31G(d,p)-calculated highest occupied molecular orbital (HOMO) and HOMO-2 orbitals of **1**. The size and grayscale contrast of the circles describe the amplitude and sign of the LCAO (linear combination of atomic orbitals) coefficients associated with the π-atomic orbitals, respectively.

Figure 2 shows an STM image of **1** at the graphite/solution interface. It reveals the formation of a crystalline monolayer architecture with the molecules face-on packed with respect to the surface. According to the resonance-enhanced tunneling model, the contrast in the current STM images is primarily determined by the energy difference between the frontier orbitals of the adsorbate and the Fermi level of the substrate.[27] For this reason, the conjugated core of our molecule exhibited a higher current than the aliphatic side chains, because of the higher tunneling probability. Therefore, in Figure 2, the core of the molecules appears brighter, because of the large coupling of its frontier orbitals with the Fermi level of the HOPG substrate, whereas the darker parts of the image can be ascribed to the aliphatic chains. The alkyl chains could not be resolved because of their high conformational mobility on the timescale of the STM measurements, probably because of steric hindrance.

The stripes observed in Figure 2 were formed by rows of molecule **1** self-assembled into dimers, with the HAT cores packed antiparallel within the dimer. This packing allowed the minimization of steric hindrance between the aromatic moieties, as already observed for various triphenylene compounds.[16,18] As a matter of fact, the outcome of molecular self-assembly on HOPG was determined by a compromise between the enthalpic gain upon molecular adsorption at the surface, the steric hindrance of the aromatic groups, and the interdigitation of the alkyl chains.[28–30]

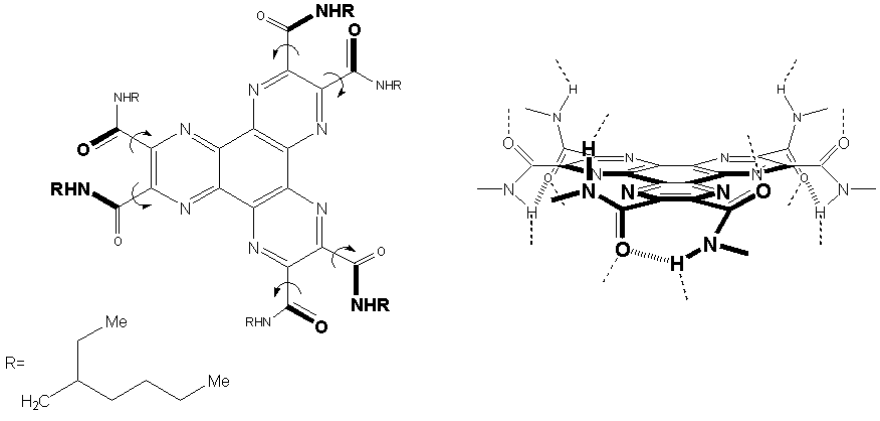

Figure 1. Chemical structure (top and side view) of the *N*-(2-ethylhexyl)-substituted hexacarboxamidohexaazatriphenylene derivative (**1**). The diameter of the aromatic core including the amide units was estimated to be ca. 1.2 nm by using theoretical modeling. The additional length of the ethylhexyl side chains was found to be roughly 0.7 nm per chain in the case where they adopted the ideal fully stretched conformation.

The unit cell of the adsorbate structure, containing two molecules, is defined by $a = (2.06 \pm 0.05)$ nm, $b = (4.38 \pm 0.07)$ nm, $\alpha = 85.4° \pm 0.7°$, and area = (8.7 ± 0.1) nm^2. A nonequivalent contrast in the STM current images is visible both among molecules belonging to the two adjacent lines that form the dimers, and among the three bright spots composing a given molecule. This is a consequence of the different environments that atoms (or groups of atoms) from each individual

molecule adsorbed on HOPG experience, because of the fact that prominent tunneling sites of bare graphite correspond to the second atom of each hexagonal lattice. Such a difference in the local STM contrast has already been reported for *n*-alkanes,[11] polycyclic aromatic hydrocarbons,[31] and triazatrinaphthylene derivatives.[32]

As already mentioned, the high spatial resolution achieved by STM imaging allowed us to resolve three bright spots in a single molecule (Fig. 2). The average distance between these spots amounted to (1.01 ± 0.07) nm. Surprisingly, this value is notably larger than the 0.42 nm estimated distance between the pyrazine rings of the molecule. The size of the highly conductive zone, which appears brighter in the image, was thus larger than that of the pure azatriphenylene core. This suggests that, under the tunneling conditions employed here, the six amide groups yielded a larger conductivity than the aliphatic parts, and thus contributed to the brighter spots together with the aromatic core of the molecule.

In order to further cast light onto this issue, quantum-chemical calculations were carried out. We first optimized the geometry of a single molecule at the Hartree–Fock level using a 6-31G(d,p) basis set. The amide substituents were initially positioned in the same plane as the central conjugated core; each long alkyl chain was replaced by a hydrogen atom because this did not affect the energy of the frontier electronic levels and did not contribute to the bright spots observed in the STM images. The results indicated that the highest occupied molecular orbital (HOMO) was doubly degenerate and localized exclusively on the conjugated HAT core. The lower-lying occupied orbitals were located about 1 eV below the HOMO level; we found a large number of electronic levels in this energy range with a strong weight on the amide substituents. The strong localization on the conjugated core as compared to the substituents is visualized in Figure 2b and c showing the shape of the HOMO and HOMO-2 levels, respectively. Similar conclusions were reached when calculating the electronic structure at the semiempirical Hartree–Fock INDO (intermediate neglect of differential overlap) level[33] on the basis of the Hartree–Fock geometry. Interestingly, the separation between the pair of amide groups (measured as the distance between the middle of the lines connecting the two oxygen atoms of the amide groups of a given branch) is about 0.9 nm, which is in agreement with the experimental distance observed between the bright spots. It thus appears that the electronic levels localized on the amide groups largely governed the pattern of the STM images; though much deeper than the HOMO with respect to the Fermi level of the substrate, these levels actually yielded a total electronic density much larger than that associated with the HOMO level. This picture was not altered when the substituents were lying out of the plane of the conjugated core and when a small graphite sheet was introduced underneath the molecule in the INDO calculations.

In order to gain insight into the electronic properties at the ensemble level, KPFM measurements[20] were performed on dry self-assembled layers of **1** on HOPG, and the local surface potential of such architectures was determined. Figure 3 displays the topography (Fig. 3a) and surface-potential image (Fig. 3b) of a film prepared by drop-casting a 5×10^{-5} mol L^{-1} solution of **1** in $CHCl_3$ on HOPG at room temperature (RT). It shows a discontinuous layer at the bottom of the image and much less adsorbate on the top. The layer thickness was determined to be $h = (1.4 \pm 0.3)$ nm. The face-on packing on HOPG found by STM suggested that these layers are four to five molecules thick, with the discotic core lying parallel to the surface. This type of packing is also in line with previously reported spectroscopic studies on thin films of a similar azatriphenylene-based compound, i.e., hexakis(hexylthio)diquinoxalino[2,3-*a*:2′,3′-*c*]phenazine, adsorbed on HOPG.[34] Even though a slight tilting of the molecules during growth cannot be excluded from consideration, a structural transition of the Stransky–Krastanov type within the film, such that the molecules of the undermost layers are oriented parallel to the substrate surface whereas the outermost layers have a different azimuthal order, can be ruled out. As a matter of fact an overlayer was observed on films of similar thickness prepared from dichlorobenzene solutions; SFM phase imaging for such samples revealed a multilayer formation characterized by a different molecular packing during the growth (image not shown). We chose to perform KPFM measurements on layers obtained from chloroform solutions, because the morphology obtained on the HOPG surface offered a good dataset consisting of coexisting uniformly thick adlayers, which do not exhibit any structural transition during growth, and an almost uncoated HOPG surface. The KPFM measurements, performed at RT in a sealed chamber filled with N_2, making use of different Pt–Ir-coated silicon tips, allowed the determination of the difference in surface potential (ΔSP) between the HOPG surface and the layer with a resolution of the order of 10 meV. HOPG was chosen as a reference substrate because its work function is well known ($\phi_{HOPG} = 4.65$ eV).[35] From profiles in the

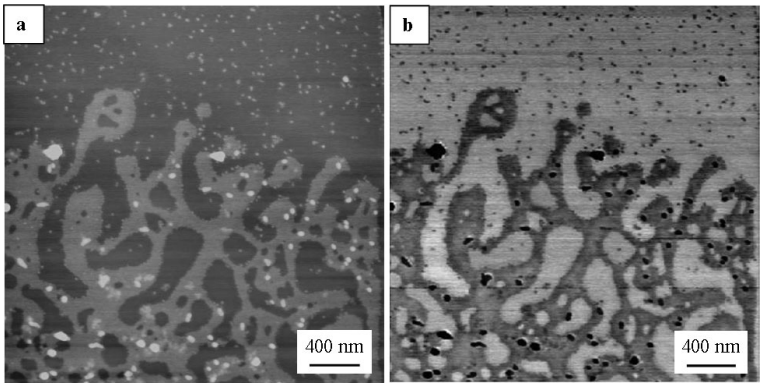

Figure 3. Discontinuous layer of **1** on HOPG: a) a topographical SFM image: whereas the adlayer of **1** appears brighter, the darker areas can be ascribed to bare HOPG; b) a KPFM image—the layer of **1** appears darker than the HOPG substrate. *Z*-scales are a) 15.0 nm and b) 231 meV.

ADVANCED MATERIALS

KPFM image, we measured $\Delta SP = SP_{HOPG} - SP_{HAT}$ to be (83.1 ± 10.3) meV. The measured surface potential of HOPG corresponds to its work function[36] and, given its value reported in the literature, the layers of **1** on HOPG exhibited a surface potential of (4.53 ± 0.02) eV. This estimation is of fundamental importance in molecular electronics because it enables the elucidation and correct tuning of differences in energy levels between molecular nanostructures and electrodes, thereby allowing optimization of charge injection. Nevertheless, it is possible that a polarization induced by the charged tip contributes to the measured surface potential.[36] Moreover, it must be kept in mind that the surface potential of a nanometer-sized molecular assembly depends on many factors, which include: the degree of electron delocalization in the π states; the molecular orientation at the surface; the molecular packing density; a possible dipole barrier at the interface between the substrate and the molecular assembly; the presence of defects in the film; and the different conformations of the aliphatic peripheral chains that might cover the conjugated core.[37] Furthermore, a variation of the electronic properties of the adsorbate induced by the substrate cannot be excluded from consideration.[27,31] Given such limitations, current activity in our laboratory is focused towards achieving control over the aforementioned factors.[36]

In summary, we have studied the structural organization and electronic properties, both at the single-molecule and ensemble level, of a specially designed and synthesized azatriphenylene. On electrically conductive substrates such as HOPG, STM investigations at the solid/liquid interface highlighted the formation of ordered monolayers with molecules assembled face-on with respect to the basal plane of the surface. The analysis of the energy levels contributing to the contrast in the current STM images, supported by quantum-chemical calculations, revealed a significant contribution of the electronic levels localized on the amide groups. Furthermore, whereas SFM provided evidence for the formation of ultrathin films on HOPG, KPFM measurements allowed us to determine the surface potential of such layers. This physical property is of fundamental importance, because the fine tuning of the difference in energy levels between molecular nanostructures and electrodes influence the rates of electron- and hole-transfer processes at metal/organic contacts, and this in turn determines the amplitude of the current through molecular junctions.[38]

Experimental

STM imaging at the solid/liquid interface was performed using commercial apparatus (multimode Nanoscope IV, Veeco). First the lattice of a freshly cleaved HOPG (001) surface (ZYH grade, advanced ceramics, USA) was examined for at least two hours until a thermal equilibrium was reached. A drop of an almost saturated solution of azatriphenylene in tetradecane was applied to the basal plane of the substrate. Then the Pt/Ir tip was immersed in the organic solution. By varying the tunneling parameters it was possible to visualize either the first organic layer physisorbed on the basal plane of the substrate or the HOPG lattice underneath. Tetradecane was chosen as a solvent as the molecule investigated exhibited sufficient solubility in it, and because its polarity and high boiling temperature assured a proper and stable environment for STM measurements at the solid/liquid interface. Phenyloctane was also employed because of its suitable properties for STM experiments at the solid/liquid interface, but with no success. This was probably because of the poor solubility of the investigated molecule in the solvent.

The STM images were recorded in constant-current mode under ambient conditions. Unit cells were averaged over several images after correction for the piezo drift making use of SPIP software (Scanning Probe Image Processor (SPIP) version 2.0 image metrology ApS, Lyngby, Denmark).

KPFM measurements were performed at RT in a sealed N_2 environment with commercial apparatus (Multimode IIIA-Veeco with Extender Electronics module). Antimony (n) doped silicon tips were used. In order to obtain sufficiently large and detectable mechanical deflections, we employed soft ($k < 4$ N m^{-1}) cantilevers with oscillating frequencies in the range ($60 < \omega < 100$) KHz (SCM, Veeco). Both sides of the cantilever were coated with 20 nm of PtIr, with a buffer layer (3 nm) of Cr to improve the adhesion. To acquire "simultaneous" SFM and KPFM images, a topographic line scan was first obtained by SFM operating in Tapping Mode, and then that same line was re-scanned in Lift Mode with the tip raised to a lift height of between 5 and 20 nm. The basic principles of KPFM have been described in detail elsewhere [20]. In brief, KPFM provides a local measure of the surface potential (SP) difference ($\Delta\phi$) between the conductive tip and the sample under investigation. SP is defined as $(\phi_{tip} - SP_{sample})/q$, where ϕ_{tip} is the work function (WF) of the tip and SP_{sample} is the SP of the sample; q is the magnitude of the elementary charge. The SP of layers of **1** is defined as $\phi + \Delta_{pol}$, where ϕ is the local work function of the nanostructure and Δ_{pol} is the polarization induced by the tip. In the performed KPFM experiments, a bias voltage $V_{tip} = V_{dc} + V_{ac} \sin\omega t$ is applied directly to the tip, holding the sample to the ground potential; ω is the resonant frequency of the cantilever, and V_{dc} and V_{ac} are a continuous and alternate bias respectively. A feedback loop continually adjusted V_{dc} to nullify the force component at frequency ω between the tip and the sample. V_{dc} was recorded as a function of the position, yielding a map of the sample SP. The calibration and the optimization of the experimental parameters were achieved using the procedure proposed by Jacobs et al [39].

Scanning probe microscopies are local probe techniques that reveal local features, which are not necessarily representative of the whole sample surface. Because of this, it is appropriate to record and process several images on different points of the sample surface. This makes it possible to minimize the influence of a particular sample area and to determine an average behavior. All the evaluations were carried out quantitatively and averaged over a large number of samples making use of two different types of image-processing software: SPIP (version 2.0), and "Nanoscope" version 6.13R1, digital instruments Veeco.

Received: June 28, 2006
Revised: September 4, 2006
Published online: November 28, 2006

[1] Special Issue on Supramolecular Approaches to Organic Electronics and Nanotechnology, *Adv. Mater.* **2006**, *18*, 1225.
[2] F. J. M. Hoeben, P. Jonkheijm, E. W. Meijer, A. Schenning, *Chem. Rev.* **2005**, *105*, 1491.
[3] B. W. Messmore, J. F. Hulvat, E. D. Sone, S. I. Stupp, *J. Am. Chem. Soc.* **2004**, *126*, 14 452.
[4] P. Samorì, *Scanning Probe Microscopies Beyond Imaging: Manipulation of Molecules and Nanostructures*, Wiley-VCH, Weinheim, Germany **2006**.
[5] A. C. Grimsdale, K. Müllen, *Angew. Chem. Int. Ed.* **2005**, *44*, 5592.
[6] A. M. van de Craats, J. M. Warman, A. Fechtenkötter, D. J. Brand, M. A. Harbison, K. Müllen, *Adv. Mater.* **1999**, *11*, 1469.
[7] A. S. Drager, R. A. P. Zangmeister, N. R. Armstrong, D. F. O'Brien, *J. Am. Chem. Soc.* **2001**, *123*, 3595.

[8] D. Adam, P. Schuhmacher, J. Simmerer, L. Haussling, K. Siemensmeyer, K. H. Etzbach, H. Ringsdorf, D. Haarer, *Nature* **1994**, *371*, 141.
[9] J. Hoogboom, P. M. L. Garcia, M. B. J. Otten, J. A. A. W. Elemans, J. Sly, S. V. Lazarenko, T. Rasing, A. E. Rowan, R. J. M. Nolte, *J. Am. Chem. Soc.* **2005**, *127*, 11 047.
[10] N. Boden, R. J. Bushby, J. Clements, B. Movaghar, *J. Mater. Chem.* **1999**, *9*, 2081.
[11] J. P. Rabe, S. Buchholz, *Science* **1991**, *253*, 424.
[12] S. De Feyter, F. C. De Schryver, *J. Phys. Chem. B* **2005**, *109*, 4290.
[13] P. Samorì, J. P. Rabe, *J. Phys.: Condens. Matter* **2002**, *14*, 9955.
[14] L.-J. Wang, *Acc. Chem. Res.* **2006**, *39*, 334.
[15] B. A. Hermann, L. J. Scherer, C. E. Housecroft, E. C. Constable, *Adv. Funct. Mater.* **2006**, *16*, 221.
[16] L. Askadskaya, C. Boeffel, J. P. Rabe, *Ber. Bunsen-Ges.* **1993**, *97*, 517.
[17] F. Charra, J. Cousty, *Phys. Rev. Lett.* **1998**, *80*, 1682.
[18] J. Wu, Q. Zeng, S. Xu, C. Wang, S. Yin, C.-L. Bai, *ChemPhysChem* **2001**, *2*, 750.
[19] T. Yatabe, M. A. Harbison, J. D. Brand, M. Wagner, K. Müllen, P. Samorì, J. P. Rabe, *J. Mater. Chem.* **2000**, *10*, 1519.
[20] V. Palermo, M. Palma, P. Samorì, *Adv. Mater.* **2006**, *18*, 145.
[21] S. Kumar, *Liq. Cryst.* **2004**, *31*, 1037.
[22] G. Kestemont, V. de Halleux, M. Lehmann, D. A. Ivanov, M. Watson, Y. H. Geerts, *Chem. Commun.* **2001**, 2074.
[23] M. Lehmann, G. Kestemont, R. G. Aspe, C. Buess-Herman, M. H. J. Koch, M. G. Debije, J. Piris, M. P. de Haas, J. M. Warman, M. D. Watson, V. Lemaur, J. Cornil, Y. H. Geerts, R. Gearba, D. A. Ivanov, *Chem. Eur. J.* **2005**, *11*, 3349.
[24] O. Roussel, G. Kestemont, J. Tant, V. de Halleux, R. Gomez Aspe, J. Levin, A. Remacle, D. Ivanov, R. I. Gearba, M. Lehmann, Y. H. Geerts, *Mol. Cryst. Liq. Cryst.* **2003**, *396*, 35.
[25] R. I. Gearba, M. Lehmann, J. Levin, D. Ivanov, M. H. J. Koch, J. Barbera, M. G. Debije, J. Piris, Y. H. Geerts, *Adv. Mater.* **2003**, *15*, 1614.
[26] V. Lemaur, A. da Silva Filho, V. Coropceanu, M. Lehmann, Y. H. Geerts, J. Piris, M. G. Debije, A. M. van de Craats, K. Senthilkumar, L. A Siebbeles, J. M. Warman, J.-L. Brédas, J. Cornil, *J. Am. Chem. Soc.* **2004**, *126*, 3271.
[27] R. Lazzaroni, A. Calderone, J.-L. Brédas, J. P. Rabe, *J. Chem. Phys.* **1997**, *107*, 99.
[28] A. Stabel, R. Heinz, F. C. De Schryver, J. P. Rabe, *J. Phys. Chem.* **1995**, *99*, 505.
[29] A. Stabel, R. Heinz, J. P. Rabe, G. Wegner, F. C. De Schryver, D. Corens, W. Dehaen, C. Sueling, *J. Phys. Chem.* **1995**, *99*, 8690.
[30] L. C. Giancarlo, G. W. Flynn, *Acc. Chem. Res.* **2000**, *33*, 491.
[31] P. Samorì, N. Severin, C. D. Simpson, K. Müllen, J. P. Rabe, *J. Am. Chem. Soc.* **2002**, *124*, 9454.
[32] N. Saettel, N. Katsonis, A. Marchenko, M. P. Teulade-Fichou, D. Fichou, *J. Mater. Chem.* **2005**, *15*, 3175.
[33] J. Ridley, M. C. Zerner, *Theor. Chim. Acta* **1973**, *32*, 111.
[34] X. Crispin, J. Cornil, R. Friedlein, K. K. Okudaira, V. Lemaur, A. Crispin, G. Kestemont, M. Lehmann, M. Fahlman, R. Lazzaroni, Y. Geerts, G. Wendin, N. Ueno, J.-L. Brédas, W. R. Salaneck, *J. Am. Chem. Soc.* **2004**, *126*, 11 889.
[35] C. Sommerhalter, T. W. Matthes, T. Glatzel, A. Jäger-Waldau, M. C. Lux-Steiner, *Appl. Phys. Lett.* **1999**, *75*, 286.
[36] A. Liscio, V. Palermo, D. Gentilini, F. Nolde, K. Müllen, P. Samorì, *Adv. Funct. Mater.* **2006**, *16*, 1407.
[37] V. Palermo, M. Palma, Z. Tomovic, M. D. Watson, R. Friedlein, K. Müllen, P. Samorì, *ChemPhysChem* **2005**, *6*, 2371.
[38] J. R. Heath, M. A. Ratner, *Phys. Today* **2003**, *May*, 43.
[39] H. O. Jacobs, H. F. Knapp, A. Stemmer, *Rev. Sci. Instrum.* **1999**, *70*, 1756.